

Enhanced velocity based pore pressure prediction using lithofacies clustering: A case study from a reservoir with complex lithology in Dezful Embayment, SW Iran

Farid ArabAmeri^a, Hamid Soleymani^{b,*}, Behzad Tokhmechi^a

^a*University of Tehran, Iran*

^b*The Graduate Center, City University of New York, U.S.A*

Abstract

The primary goal of this paper is to improve accuracy and reliability of the conventional Bowers and Tau methods in a reservoir with complex lithology. We demonstrate the capability of the proposed method through a case study in a reservoir in the Southwest of Iran. Velocity based pore pressure prediction methods are widely accepted as a routine technique in the petroleum industry. Despite recent improvements, still, literature suffer from inconsistencies and uncertainties mostly arise from velocity anomalies due to complex lithostratigraphic setting or presence of various formation fluids. Our proposed workflow aims to address those issues and improve the accuracy of the estimations by clustering the input data into zones with specific geomechanical characteristics. We hypothesis each major zones at the offset test wells might have distinct "Normal Compaction Trend" with a different empirical constants. Thus, Bowers and Tau methods should be calibrated for each cluster rather the whole stratigraphic column. The clustering task was done by statistical analyses of a suite of well logs and validated with core derived lithologies. Several clustering techniques namely K-means, basic sequential algorithmic scheme, single, and complete linkage hierarchical were applied and compared to find the best algorithm. We found that the self-organizing map (SOM) method provide the best results by maximizing lithology likelihood within each cluster and improve the efficiency of the Bowers and Tau methods. Satisfactory results of this study offer a safe ground for implementation of the proposed method in other sedimentary basins.

Keywords: Pore Pressure, Bowers Method, Tau Method, Self-Organizing Map, Lithofacies

1. Introduction

Pore pressure prediction is an active and longstanding research area in the Earth science, and it has been the focus of the petroleum industry since the early days of exploration and exploitation. Blowouts, kicks, borehole washouts, wellbore breakout and stuck pipe

*Corresponding author

Email addresses: farid.ameri@alumni.ut.ac.ir (Farid ArabAmeri),
hsolyemani@gradcenter.cuny.edu (Hamid Soleymani), tokhmechi@ut.ac.ir (Behzad Tokhmechi)

(Oughton et al., 2015) are just number of issues that may occur while encountering unexpected fluid pressure anomalies during drilling. To reduce the associated risks of drilling a robust mud plan and casing design is required as a part of every drilling operation (Nguyen et al., 2015; Wild et al., 2015). Today a reliable estimate of pore pressure before drilling is not just a routine to increase safety and cost efficiency of the operation, but it also provides an unparalleled source of information in the exploration phase. Pore pressure data can be used to inform suitable production method, maximum hydrocarbon column in the reservoir, integrity and sealing capacity of the caprock, and its economic threshold (Holm, 1998; Hao et al., 2015; Guglielmi et al., 2015; Cranganu and Soleymani, 2015; Cranganu et al., 2014).

One of the remarkable early contributions in the estimation of pore pressure was made by Hottmann et al. (1965). They documented that the porosity decrease as a function of depth in sediments from the southern Louisiana gulf coast and by extension, applied their observations to other sedimentary basins. They further state that any deviations from the normal trend could be associated with abnormal pore pressure. Eaton et al. (1972) showed the application of deep resistivity log data in shale sediments of the Gulf of Mexico as an indicator of higher pore pressure. He also introduced an empirical equation to derive pore pressure by demonstrating the relationship between effective stress and sonic-transit-time. Bowers et al. (1995) proposed a power law relationship between compressional velocity and effective stress by calculating the overburden stress and measured pore pressure at well locations. Similarly, Giles et al. (1998) introduced a compound mudline and matrix-transit-time variable (Tau) in a first-order effective stress-velocity power relationship. Later, Boitnott et al. (2009) improved Bowers method by considering a normal compaction trend that is asymptotic to matrix velocities and can provide a better representation of the physical properties of the rocks. One should keep in mind that above methods are heavily reliant on the relationship between porosity and pore pressure (Mannon and Young, 2017) which may not be a valid assumption in case of complex lithology.

Generally, velocity based pore pressure prediction methods follow three routine procedures: (1) acquiring, editing, and processing sonic logs or seismic velocity data; (2) calibrating velocity and effective stress, using a proper regression model at offset wells; (3) calculating pore pressure at a new well location using the calibrated relationship (Wang et al., 2015). Various authors reported a successful application of integrated velocity data by incorporating various available velocity sources (e.g., sonic logs, seismic velocity) to estimate pore pressure (Riahi and Soleymani, 2011; Soleymani and Riahi, 2012; Liu et al., 2018). However, generating a comprehensive velocity model compound of various type of data is not straightforward. For instance, presence of a secondary phases (e.g., methane, brine) introduce a major uncertainty and may lead to false interpretation of the velocity data and inaccurate pore pressure estimation (Nour and AlBinHassan, 2013). Accurate calibration of Bowers or Tau relationships for a specific geological setting is an essential step in velocity based pore pressure estimation (Sheng et al., 2017), and it can reduce the associated uncertainties significantly.

2. Geological framework

The studied oil field is located in the Southwest of Iran in Dezful embayment and follows the northwest-southeast trend of Zagros. It consists of five major formations namely Aghajari, Mishan, Gachsaran, Asmari (productive reservoir), and Pabdeh. Investigating lateral lithology variations and complex stratigraphy of the Asmari formation throughout the basin is the focus of this study, and it is a major challenge for drilling companies. A comprehensive study by [Van Buchem et al. \(2010\)](#) indicated that the OligoceneMiocene Asmari formation mostly consists of shallow-water carbonate depositions and siliciclastics. While Sandstones are deposited as sheets on top of the carbonate platform as lobes or bars along the margins of the intrashelf basin or as turbidites in the basin center, the carbonates are mostly formed in the platform margin and can be massive and grainy and form prograding clinoforms. The reservoir also has a complex stratigraphic architecture, which consists of three Oligocene and three Miocene sequences. "Stratigraphic architecture of these sequences is primarily controlled by glacio-eustatic sea-level fluctuations, which has determined the distribution of carbonates, sandstones, and anhydrites" ([Van Buchem et al., 2010](#)). These different rock types were formed in low- to high-energy homoclinal ramp environments ([Kangazian and Pasandideh, 2016](#)). Major depositional environments include tidal-flat, lagoonal shoal, semi-restricted and open-marine was formed along the foreland basin during the collision of Arabian plate and Iranian micro-continent ([figure 1](#)). It appears that lithological heterogeneity, complex geometries, early and late diagenetic alterations have cause Asmari formation to be considered a complex formation ([Van Buchem et al., 2010](#)). These changes reflect the dynamics of platform progradation in the reservoir ([Ehrenberg et al., 2007](#)).

Overall the reservoir can be divided into eight zones and sixteen subzones based on lithology and variations of porosity determined by neutron porosity, density, gamma ray well logs, and cores. Petrographic analysis of core samples and lithofacies studies confirm the periodic occurrence of limestone, dolomite, sandstone, and shale. The first member mostly consists of carbonates, second, third, fourth, and the fifth are mostly consist of sandstones, the sixth member consists of limestone, dolomite, and shale, the seventh member consists of limestone, sandstone, and shale, while, the eighth member consists of limestone and shale ([figure 2](#)). Anhydrite is mostly present in pore spaces of the fifth member while they could also be observed in some sandstone and carbonate members. Consolidation of sandstones in member two and three is generally better on the west side of the reservoir than its east side. Shale interlayers are also present in sandstone members, especially in top and bottom of the member three. Cross plot of V_p versus density and various members of the reservoir shows strong positive correlation ([figure 3](#)). Also, each member were showed up as a relatively distinct cluster in plots of P-wave velocity versus density.

3. Material and methods

The available dataset consists of post-stack 3D seismic with 2041 in-lines and 552 cross-lines with the spatial resolution of 25 m in in-line and cross-line directions and temporal resolution of 4 m sec. We also had access to processing information including stacking velocities, interpretation of major reflectors, seismic wavelet and acoustic impedance inversion.

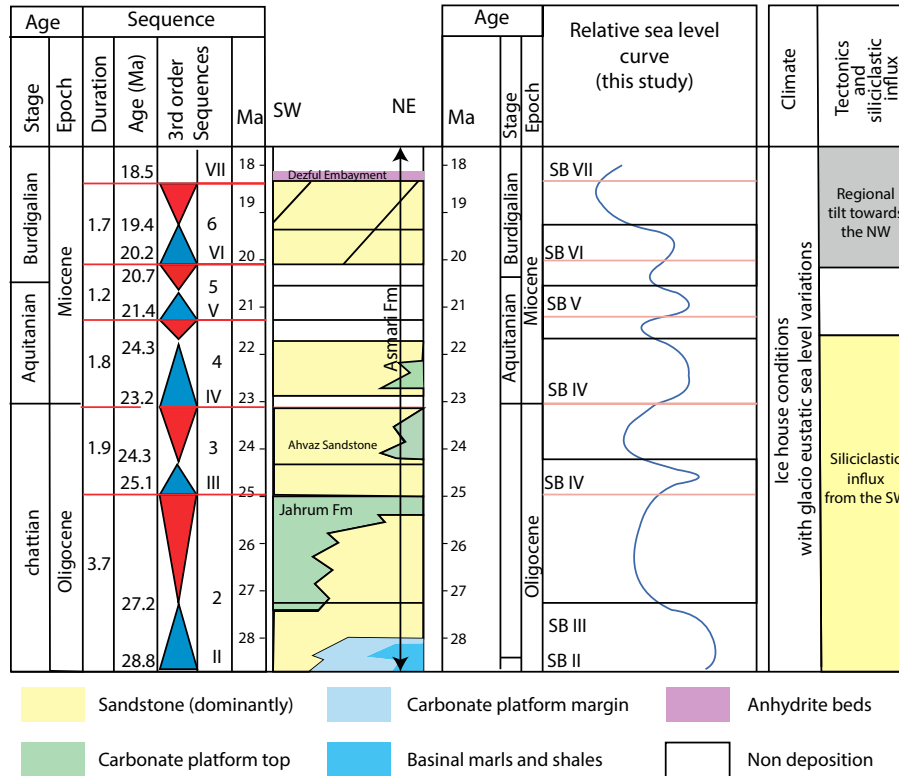


Figure 1: Van Buchem et al. (2010) described the chronostratigraphic scheme and sequence stratigraphic organization, with relative hiatuses and interpreted sea-level curve. They also documented that "the studied interval is strongly influenced by the transition from a green-house climate to an ice-house climate which occurred at the Eocene/Oligocene boundary, and which subsequently controlled sedimentation by high amplitude glacio-eustatic sea-level fluctuations (figure modified from Van Buchem et al., 2010)."

Well data was consist of the complete suite of well logs including density, electrode resistivity devices (LLD, LLS, MSFL), gamma ray, neutron porosity, compressional velocity, photoelectric absorption factor (PEF data was not available for all wells), and caliper measurements. Downhole measurements including repetitive formation test (RFT), core measurements including special core analysis (SCAL), and X-ray powder diffraction (XRD) were available at few well locations (figure 2).

Petrographic data were obtained from X-ray powder diffraction (XRD) analysis of the core samples and suit of available well logs. Final velocity, density, and porosity information were upscaled in the respective cells of an integrated finite element geologic model that were generated by using available seismic data and suit of well logs.

Five clustering techniques including, complete and single linkage hierarchical, K-means, and basic sequential algorithmic scheme were applied to well logs and core data to find the best algorithm that can classify the reservoir column based on the present lithology. Similar routine adopted previously by various workers mainly to reduce the uncertainties associated with sharp lithology variations. Igbokwe (2011) clustered well logs to interpret

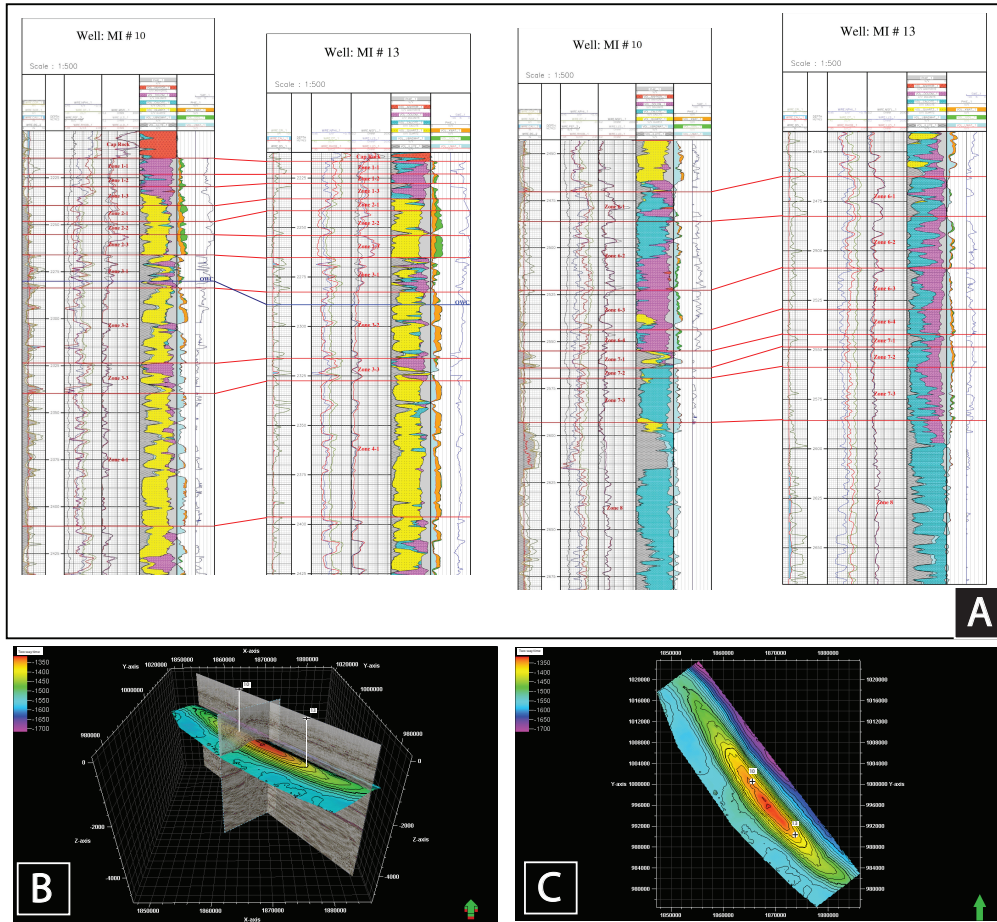


Figure 2: Composite log of well logs, major zones and mineralogy observations along with 3D seismic data and interpretation of the top of the Asmari formation. Various zones and sub-zones of the Asmari formation were interpreted and shown on the well logs using probabilistic analysis and core measurements (A). 3D view of the interpreted map of the top of Asmari formation along with the selected well locations (B). 2D view of the top of the Asmari formation with the location of the selected wells (C).

stratigraphy of Canadian Peace River oil sand into homogeneous lithofacies intervals; Zhou et al. (2017) predicted pore pressure by dividing the sonic log data into homogeneous sections in Appalachia basin. Al Ibrahim et al. (2017) also utilized cluster analysis of well logs using SOM and hierarchical clustering for multi-scale lithofacies analysis in carbonates of Hanifa formation in Saudi Arabia.

We conclude that the self-organizing map (SOM) provides the best results by maximizing lithology likelihood within each cluster and improves the efficiency of the Bowers and Tau methods. The calibrated effective-stress velocity relationship for lithologically homogeneous zones was used to calculate pore pressure.

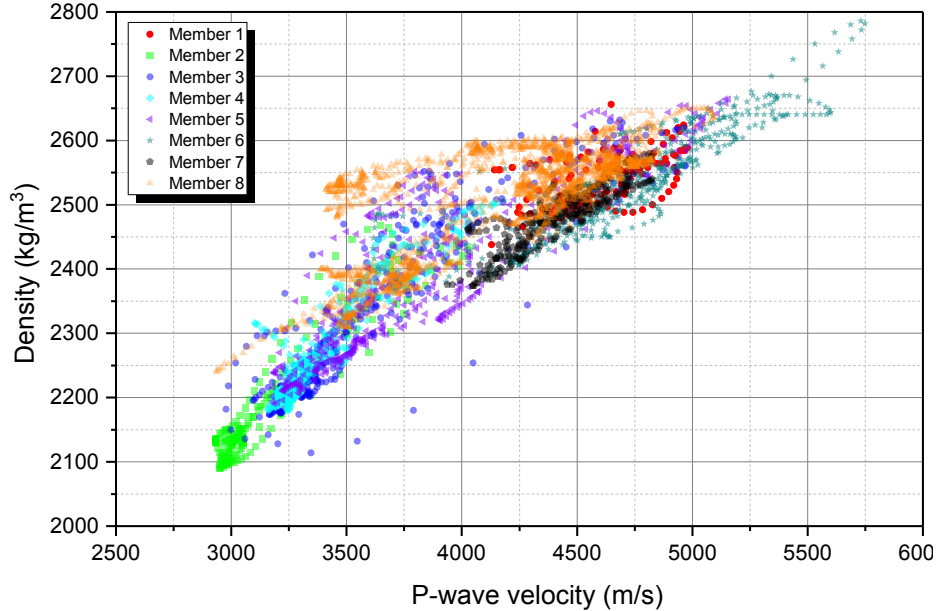


Figure 3: Relatively distinct spread of various members (classified based on age and microfossil studie) suggests the presence of distinct lithological units within the data. Also, note the strong positive correlation between P-wave velocity and density with color-coded members at a selected well location.

4. Theory

4.1. Self-organizing maps clustering

The SOM clustering is a well-known unsupervised learning method in the family of artificial neural networks (Kohonen, 1998). Various workers document the geophysical application of the SOM. As an early adopter Coléou et al. (2003) used it as a tool in seismic interpretation and called it “an essential tools for unsupervised seismic analysis.” Similarly, other scholars benefit from SOM method in the seismic-facies analysis (Saraswat and Sen, 2012) and recognition of seismic patterns (Kourki and Riahi, 2014; Yang et al., 1991). Jouini and Keskes (2017) utilized the SOM in characterizing mechanical properties of the reservoir rocks. Sfidari et al. (2014) demonstrated that SOM could provide much better results for lithofacies clustering than other clustering methods.

A notable advantage of this method is preserving the topology of high dimensional space by mapping the initial data set into a two-dimensional space with the rectangular or hexagonal structure of weighted neurons (Kohonen and Somervuo, 2002). During the first iterations, weights are either allocated to neurons randomly, or through sampling the generated principal component eigenvectors of the subspace. Then, the Euclidean distance between the provided input and the weight vectors are measured, and the nearest neuron will be selected. The selected neuron and other neurons in its neighborhood will alter to become as similar as the input vector. Through multiple iterations, the weights of the neurons converge as the neighborhood of the best matching unit (BMU) shrinks (Ciampi and Lechevallier, 2000). The robustness of SOM clustering method could be associated with its characterized non-

linear projection from the higher dimensional space of inputs to a low dimensional grid, which facilitates the discovery of hidden patterns in the input data (Kohonen and Honkela, 2007; Moghimdarzi et al., 2016). The SOM proved to be able to handle large noisy datasets effectively (Shahreza et al., 2011; Oyana et al., 2012), and it has been applied successfully in complex structures (Tasdemir and Merényi, 2009).

4.2. Modified basic sequential algorithmic scheme

In the modified basic sequential algorithmic scheme (M-BSAS), each cluster is represented by mean of the assigned vector (Ahmadi and Berangi, 2008). The algorithm calculates the distance between each data point and the cluster centroid. While the maximum number of clusters has not been reached and if the distance was larger than a pre-defined threshold of dissimilarity, a new cluster will be formed, and the data point will be assigned to the nearest cluster (Theodoridis et al., 2010). Note that the method is heavily dependent on the order of presenting data and user-defined threshold. The mean vector for clusters will be updated as:

$$m_{C_k}^{new} = \frac{(n_{C_k}^{new} - 1)m_{C_k}^{old} + x}{n_{C_k}^{new}} \quad 1$$

where x is the value of the new data, C_k is cluster center, and $n_{C_k}^{new}$ is the cardinality of C_k after x assignment. The algorithm consists of two phases; firstly, some of the data are presented to determine the maximum number of clusters. Secondly, the unassigned data are allocated to their appropriate clusters (Kainulainen and Kainulainen, 2002). Sarparandeh and Hezarkhani (2016) implemented this method for delineating lithology and exploring rare elements. Jin (1994) also implemented BSAS for two-dimensional subsidence analysis.

4.3. K-means

This algorithm uses k pre-defined number of clusters from a set of n , d-dimensional data points with the objective of minimizing the Euclidean distance between cluster centers and data points (Hong et al., 2017). The underlying algorithm works by allocating each data point to the nearest cluster, then introduces new centers for each cluster. Mathematically we can write this as:

$$S_i^{(t)} = \left\{ x_p : \|x_p - m_i^{(t)}\|^2 \leq \|x_p - m_j^{(t)}\|^2 \quad \forall j, 1 \leq j \leq k \right\} \quad 2$$

where x_p is the value of the new data, $m_i^{(t)}$ and $m_j^{(t)}$ are the center of the clusters and defined as:

$$m_i^{t+1} = \frac{1}{|S_i^t|} \sum_{x_j \in S_i^t} x_j \quad 3$$

where S_i is the number of data.

These iterations continue until centroids no longer change (Reddy et al., 2012). Di Giuseppe et al. (2014), successfully utilized k-means algorithm to distinguish geological structures with

different rheologies. [Wohlberg et al. \(2006\)](#) also showed that k-means is a robust tool for delineating geological features.

4.4. Single linkage and complete linkage hierarchy

These methods belong to a distinctive type of hierarchical clustering called agglomerative. In this method, each data point is considered as a cluster ([Fouedjio, 2016](#)). In each iteration, the distance between the two clusters is calculated, and the two clusters with the nearest distance merge. This process continues until the pre-defined number of clusters are obtained ([Carlsson et al., 2017](#)). Another notable technique of this family is the complete linkage method which is different from single linkage in calculating the distance. While in single linkage method the two clusters with the closest members have the smallest distance ([equation 4](#)), in complete linkage method, the largest dissimilarity between two identical features of two data points is calculated ([equation 5](#)) ([Fouedjio, 2016](#)). Mathematically we can define:

$$d_{single}(G, H) = \min d_{ij}, i \in G, j \in H \quad 4$$

$$d_{complete}(G, H) = \max d_{ij}, i \in G, j \in H \quad 5$$

where $d_{i,j}$ is the distance between elements $i \in G$ and $j \in Y$, and G and H are two sets of elements (i.e., clusters).

4.5. Pore pressure prediction

[Bowers et al.\(1995\)](#) proposed, a drop in sonic velocity without decreasing the bulk density might be an indicator of unloading, and this phenomenon might be a direct result of fluid expansion. They also derived the effective stress from measured pore pressure data and calculate overburden stress based on sonic interval velocities from well log data in the Gulf of Mexico. They further showed that the sonic velocity and effective stress have following power law relationship:

$$V_p = V_0 + A\sigma_{eff}^B \quad 6$$

where V_p is compressional velocity at a given depth, V_0 is compressional velocity in mudline or unconsolidated saturated surface sediments, A and B are empirical constants calibrated with offset velocity versus effective stress data ([Chopra and Huffman, 2006](#)). Considering [equation 6](#), pore pressure could be calculated using the equation below ([Terzaghi, 1925](#)):

$$P_p = \sigma_o - \sigma_e \quad 7$$

where σ_o is overburden stress and σ_e is effective stress. ([Giles et al., 1998](#)) introduced new parameter τ and linked the velocity to effective stress via empirical constants as:

$$\sigma_e = A\tau^B \quad 8$$

where A and B are the fitting constants and can be calculated from [equation 9](#):

$$\tau = \frac{C - \Delta t}{\Delta t - D} \quad 9$$

where Δt is the compressional transit time, acquired from a sonic well log or seismic velocities. C is the constant related to the mudline transit time and D is constant related to matrix transit time. To use this method, one must calculate the matrix and mud-line transit times and obtain empirical constants (A and B). Mud-line transit time can also express as the transit time in saturated unconsolidated sediments in the surface (Zhang, 2011; Ugwu, 2015).

5. Enhanced pore pressure prediction

Variation of rock velocities because of lithology, porosity, gas presence, and fluid content can distort the results of conventional Bowers and Tau methods. Therefore, interpretation of any derived parameters based on velocity data requires a detailed understanding of the present lithology and fluid content. In the studied reservoir, the interplay of diverse lithostratigraphic units is the major complication in using conventional protocols. We demonstrate the poor performance of the conventional Bowers and Tau method in the studied reservoir and provide an alternative solution to increase the accuracy of the estimations.

5.1. Conventional Bowers and Tau methods

We calibrate the Bowers relationship (equation 6) in offset wells via regression analysis of the calculated effective stress at depths with available P-wave velocity (figure 4A). The results of the regression analysis of the effective stress data versus velocity confirm that the Bowers calibration is not statistically significant. Thus, calculating pore pressure based on the derived relationship will result in introducing a major uncertainty. Alternatively, we applied Tau method (equation 8) on the same dataset, and we concluded that the regression results were also not statistically significant (figure 4B). We associate this weak correlation with sharp lithology transitions in relatively small intervals which can severely reduce the accuracy of the conventional velocity based methods and lead to false interpretation.

5.2. Enhanced pore pressure prediction

To reduce the uncertainties associated with the effect of transient lithology on velocity, we derived various major lithological units in the reservoir column using multiple statistical clustering methods and applied the Tau, and Bowers methods on derived units individually. The advantage of multivariable clustering methods is providing a comprehensive basis to classify multi-dimensional dataset (e.g., well logs, core data, seismic). Five clustering methods namely; complete linkage hierarchical, K-means, basic sequential algorithmic scheme, and single linkage hierarchical were applied on well logs (i.e., density, gamma ray, neutron porosity and sonic) and the accuracy of recognizing different lithologies were analyzed by comparing the results with data obtained from cores. A metric that we used to compare the performance of the various clustering methods was their ability to recognize independent effective-stress velocity trends (i.e., R-squared of the regression trend). The summary

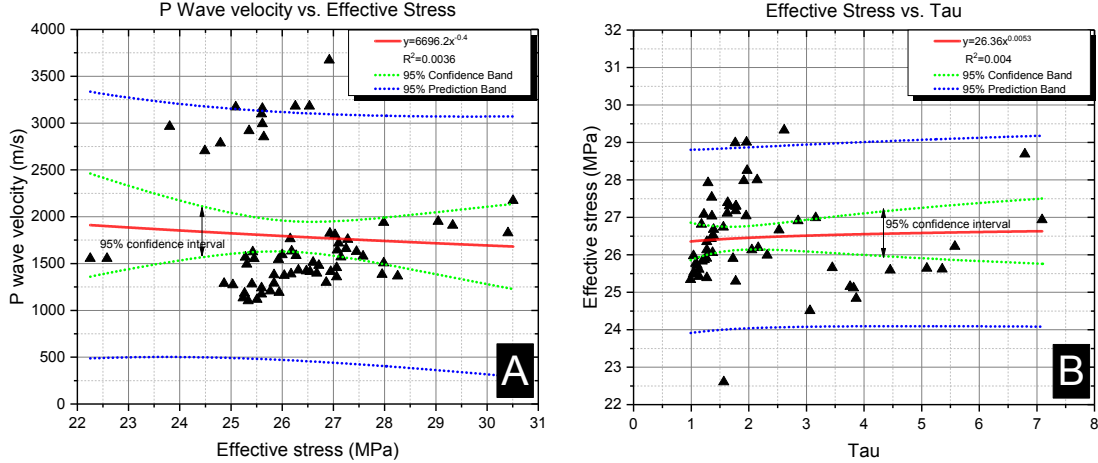


Figure 4: Effective stress vs. velocity for available well data. Bowers (A) and Tau (B) method does not provide a suitable fit, and the regression is not statistically representative of the data.

of the optimum cluster number and overall performance for different clustering algorithms is provided in [table 1](#). Although each cluster can be associated with a particular lithology, however, interpretation of well logs suggest each unit comprised of the specific lithology along with the small percentage of other units. We interpret these units as a thin layer within the major members (see [section 2](#)).

Algorithm	Performance ranking	Optimum clusters
SOM	1	5
K-means	2	7
M-BSAS	3	6
complete linkage hierarchical	4	3
single linkage hierarchical	5	4

Table 1: performance ranking for different clustering methods based on their capability to delineate lithological units and their respective optimum number of clusters.

Analysis of various clustering methods indicates that SOM provides better results in terms of delineating various lithologies compare to other previously mentioned techniques. To implement the SOM clustering algorithm and calibrate Bowers and Tau methods, we ran the clustering analysis on all available wells. The SOM algorithm was trained with weight and bias learning rules, and the mean-squared-error calculated as a metric to measure the reliability of training. Sensitivity analysis was carried out to determine the optimum number of nodes and iterations ([figure 5](#)). [Figure 5A](#) shows the quantization error decreases remarkably with increasing number of nodes. Similarly, the topological error decreases slightly and stabilize by increasing number of nodes. [Figure 5B](#) demonstrates the changes in topological and quantization error as a function of iteration. This figure also shows the quantization error decreases significantly with the number of iteration (especially within the first 400

iterations) while topological error decreases marginally. We also generated the neighbor weight distance map to obtain the optimum number of clusters. To validate the results, core samples with XRD measurements were selected, and compared with the correspondent lithologies derived from a cluster at the same depth. The selected cluster and the respective lithology information used to validate other clusters in available wells. Table 2 summarize the dominant lithology in each cluster.

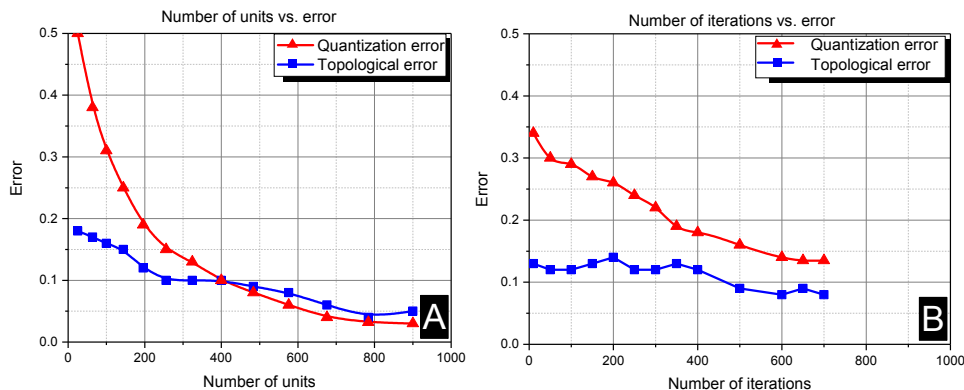


Figure 5: Quantization error and topological error variation versus number of units (A) and number of iterations (B).

Cluster #	Lithology type
1	Shale
2	Dolomite and Limestone
3	Shale and Shaly Limestone
4	Sandstone
5	Shaly Sandstone

Table 2: SOM clusters and their respective lithologies.

To calculate pore pressure with respect to new clusters, effective-stress versus velocity graphs were created for each cluster. However, due to lack of RFT data in cluster three and five, power regression fit was applied only to cluster one, two and four. We also observed relatively high velocities in cluster one along with high electrical resistivity and low porosity (figure 6). Base on these observations we conclude these shale units are highly siliceous with low clay content (less than 45% based on a gamma-ray log) (Nelson, 2010).

Figure 7 shows regression results for cluster one, two and four. To obtain a continuous prediction model within the reservoir, effective-stress versus velocity equation of cluster three and five were obtained from other clusters with similar lithology. Effective stress versus velocity trends and similarity analysis of the well logs in different clusters show that the cluster five is relatively similar to cluster two and cluster three is relatively similar to cluster four. Figure 9A demonstrates the final pore pressure estimation for all clusters (red curve) along with measured RFT.

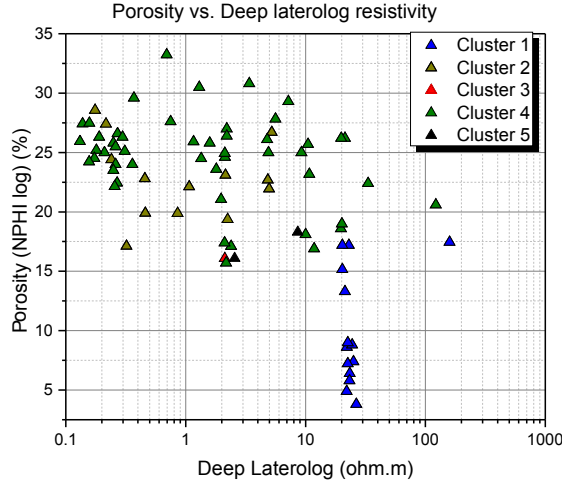


Figure 6: Cluster one shows notably low porosity and high resistivity compared to other clusters. The porosity and resistivity characteristics of the cluster one could be an indicator of high amounts of silica minerals in the overall mineralogy of the unit.

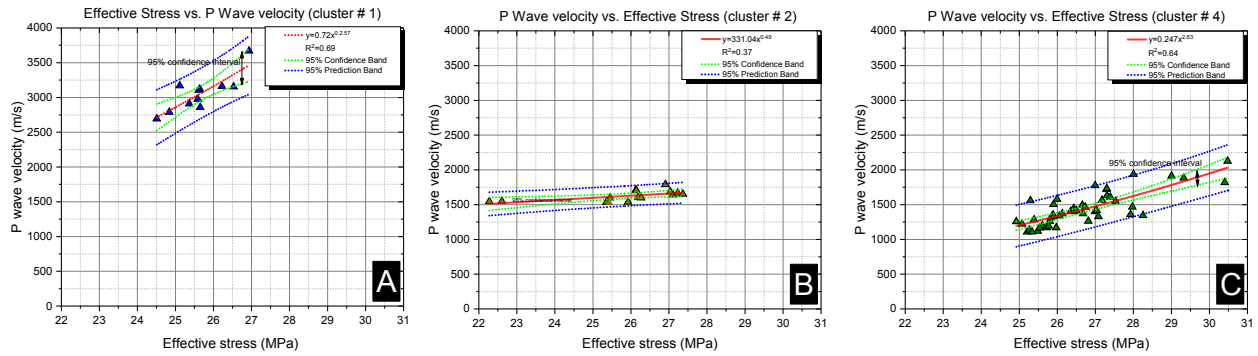


Figure 7: Regression analysis for effective stress versus $V_p - V_0$ ($V_0 \approx 1720 \text{ m s}^{-1}$) for cluster one (A), two (B), and four (C).

Tau method was also applied to the same clusters, and the regression results are shown in figure 8A, B, and C for clusters two and four respectively. Estimated pore pressure at a test well is also shown in figure 9B.

Apart from the lithology variations, another source of uncertainties that can affect the final pore pressure estimation is limited data in the formations above the reservoir, and incorrect well log values in the reservoir. The goodness of Bowers and Tau calibration regressions (R-squared) in the modified method (figure 7 and 8) suggest a significant improvement in cluster one (mostly shale) and four (mostly sandstone), while it failed to deliver the same results in cluster two (dolomite and limestone). These observations are in agreement with the principal assumption of the Bowers and Tau methods, indicating these techniques are most reliable in shale and sandstone (with lower degree of certainty compared to shales), but they do not produce reliable results in carbonate settings.

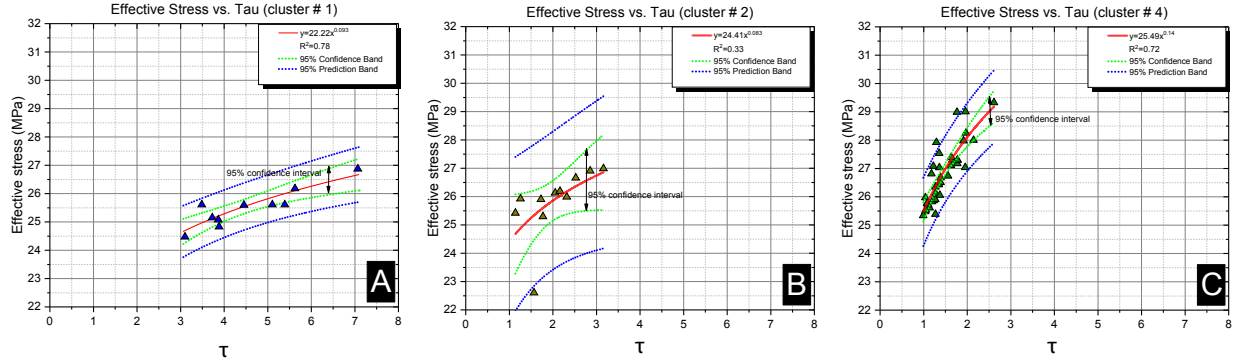


Figure 8: Regression analysis for Tau versus effective stress for cluster one (A), two (B), and four (C).

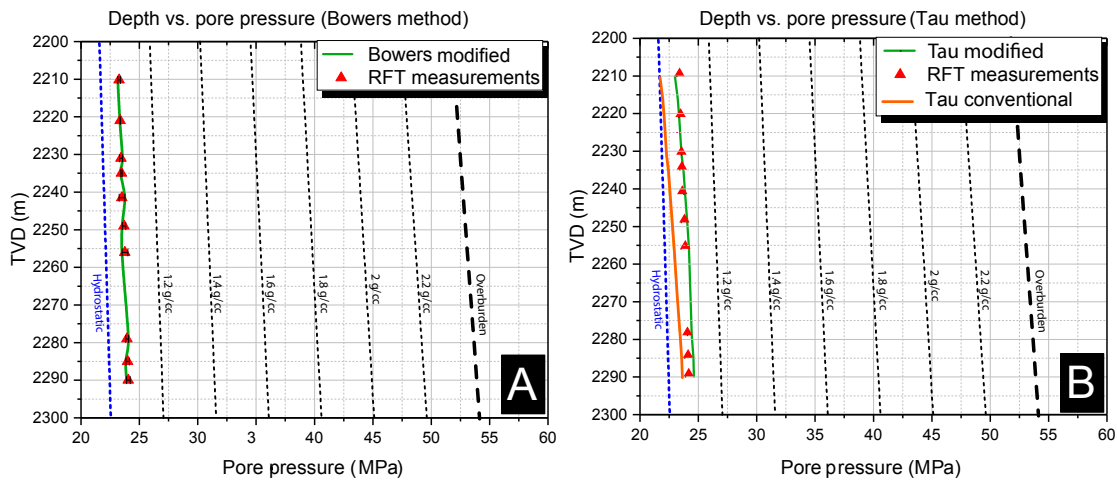


Figure 9: Pore pressure prediction based on Tau, and Bowers method along with the RFT measurements at a selected well location. (A) Modified Bowers produced a relatively accurate predictions while extremely poor calibration of the Bowers made the estimation unreliable. (B) Comparing the conventional and modified Tau method show that the later improved the accuracy of the estimation.

Overall, comparing the conventional methods with proposed procedure shows significant improvement in pore pressure estimations. Table 3 summarized the quantitative comparison (MAPE and MSE) between conventional and proposed Tau methods.

6. Conclusions

Interpretation of the estimated pore pressure using velocity based methods (i.e., Eaton and Bowers methods) is not straightforward and require a clear understanding of the lithology and geomechanical state of the reservoir. Also, inaccurate calibration of the effective stress versus velocity especially, in a reservoir with complex lithology will introduce significant uncertainty in the final estimation. In this research we showed each major zones at the offset test wells have distinct "Normal Compaction Trend" with a different empirical constants. Also, the SOM clustering algorithm is a suitable algorithm for lithofacies classification of the

Method	MAPE %	MSE
Conventional Bowers	105	146
Bowers with proposed modifications	15.5	0.76
Conventional Tau	4	21761
Tau with proposed modifications	1	1840

Table 3: Comparing Tau methods with the results of the SOM improved estimations. Mean absolute percentage error and mean square error used as a measure of the accuracy of the predictions.

log data. We conclude that in case of complex lithology the accuracy of the conventional Bowers and Tau methods can be improved by accurate calibration of the empirical equations for major lithostratigraphic units, leading to a reliable final pore pressure estimation.

Acknowledgments

The authors would like to thank S. Seyedali and A. Ahmadi for his major technical advice and many useful discussions. The authors are grateful to Iranian Offshore Oil Company (IOOC) for permission to use the seismic data and well logs.

References

- Ahmadi, N., Berangi, R., 2008. Modulation classification of qam and psk from their constellation using genetic algorithm and hierarchical clustering. In: Information and Communication Technologies: From Theory to Applications, 2008. ICTTA 2008. 3rd International Conference on. IEEE, pp. 1–5.
- Al Ibrahim, M. A., Sarg, J. F., Hurley, N., Cantrell, D. L., Humphrey, J. D., 2017. Depositional environments and sequence stratigraphy of carbonate mudrocks using conventional geologic observations, multiscale electrofacies visualization, and geochemical analysis: The case of the tuwaiq mountain and hanifa formations in a basinal setting, saudi arabia. AAPG Bulletin 101 (5), 683–714.
- Boitnott, G., Miller, T., Shafer, J., 2009. Pore pressure effects and permeability: effective stress issues for high pressure reservoirs. In: Proceedings of the International Symposium of the Society of Core Analysts (SCA’09). p. 9.
- Bowers, G. L., et al., 1995. Pore pressure estimation from velocity data: Accounting for overpressure mechanisms besides undercompaction. SPE Drilling & Completion 10 (02), 89–95.
- Carlsson, G., Mémoli, F., Ribeiro, A., Segarra, S., 2017. Admissible hierarchical clustering methods and algorithms for asymmetric networks. IEEE Transactions on Signal and Information Processing over Networks 3 (4), 711–727.

- Chopra, S., Huffman, A. R., 2006. Velocity determination for pore-pressure prediction. *The Leading Edge* 25 (12), 1502–1515.
- Ciampi, A., Lechevallier, Y., 2000. Clustering large, multi-level data sets: an approach based on kohonen self organizing maps. In: *European Conference on Principles of Data Mining and Knowledge Discovery*. Springer, pp. 353–358.
- Coléou, T., Poupon, M., Azbel, K., 2003. Unsupervised seismic facies classification: A review and comparison of techniques and implementation. *The Leading Edge* 22 (10), 942–953.
- Cranganu, C., Soleymani, H., 2015. Carbon dioxide sealing capacity: Textural or compositional controls? a case study from the oklahoma panhandle. *AAPG/DEG Environmental Geosciences* 22 (2), 57–74.
- Cranganu, C., Soleymani, H., Azad, S., Watson, K., 2014. Carbon dioxide sealing capacity: Textural or compositional controls? *AAPG Search and Discovery Article#* 41474.
- Di Giuseppe, M. G., Troiano, A., Troise, C., De Natale, G., 2014. k-means clustering as tool for multivariate geophysical data analysis. an application to shallow fault zone imaging. *Journal of Applied Geophysics* 101, 108–115.
- Eaton, B. A., et al., 1972. The effect of overburden stress on geopressure prediction from well logs. *Journal of Petroleum Technology* 24 (08), 929–934.
- Ehrenberg, S., Nadeau, P., Aqrabi, A., 2007. A comparison of khuff and arab reservoir potential throughout the middle east. *AAPG bulletin* 91 (3), 275–286.
- Fouedjio, F., 2016. A hierarchical clustering method for multivariate geostatistical data. *Spatial Statistics* 18, 333–351.
- Giles, M., Indrelid, S., James, D., 1998. Compaction the great unknown in basin modelling. *Geological Society, London, Special Publications* 141 (1), 15–43.
- Guglielmi, Y., Cappa, F., Avouac, J.-P., Henry, P., Elsworth, D., 2015. Seismicity triggered by fluid injection–induced aseismic slip. *Science* 348 (6240), 1224–1226.
- Hao, F., Zhu, W., Zou, H., Li, P., 2015. Factors controlling petroleum accumulation and leakage in overpressured reservoirs. *AAPG Bulletin* 99 (5), 831–858.
- Holm, G., 1998. How abnormal pressures affect hydrocarbon exploration, exploitation. *Oil and Gas Journal* 96, 79–84.
- Hong, S., Kumar, D. P., Reddy, D. A., Choi, J., Kim, T. K., 2017. Excellent photocatalytic hydrogen production over cds nanorods via using noble metal-free copper molybdenum sulfide (Cu₂MoS₄) nanosheets as co-catalysts. *Applied Surface Science* 396, 421–429.
- Hottmann, C., Johnson, R., et al., 1965. Estimation of formation pressures from log-derived shale properties. *Journal of Petroleum Technology* 17 (06), 717–722.

- Igbokwe, O. A., 2011. Stratigraphic interpretation of well-log data of the athabasca oil sands of alberta canada through pattern recognition and artificial intelligence. Ph.D. thesis.
- Jin, J., 1994. Bsas: a basic program for two-dimensional subsidence analysis in sedimentary basins. *Computers & Geosciences* 20 (9), 1329–1345.
- Jouini, M. S., Keskes, N., 2017. Numerical estimation of rock properties and textural facies classification of core samples using x-ray computed tomography images. *Applied Mathematical Modelling* 41, 562–581.
- Kainulainen, J., Kainulainen, J. J., 2002. Clustering algorithms: basics and visualization. Helsinki University of Technology, Laboratory of Computer and Information Science.
- Kangazian, A., Pasandideh, M., 2016. Sedimentary environment and sequence stratigraphy of the asmari formation at khaviz anticline, zagros mountains, southwest iran. *Open Journal of Geology* 6 (02), 87.
- Kohonen, T., 1998. The self-organizing map. *Neurocomputing* 21 (1-3), 1–6.
- Kohonen, T., Honkela, T., 2007. Kohonen network. *Scholarpedia* 2 (1), 1568.
- Kohonen, T., Somervuo, P., 2002. How to make large self-organizing maps for nonvectorial data. *Neural networks* 15 (8-9), 945–952.
- Kourki, M., Riahi, M. A., 2014. Seismic facies analysis from pre-stack data using self-organizing maps. *Journal of Geophysics and Engineering* 11 (6), 065005.
- Liu, L., Shen, G., Wang, Z., Yang, H., Han, H., Cheng, Y., 2018. Abnormal formation velocities and applications to pore pressure prediction. *Journal of Applied Geophysics*.
- Mannon, T., Young, R., 2017. Pre-drill pore pressure modelling and post-well analysis using seismic interval velocity and seismic frequency-based methodologies: A deepwater well case study from mississippi canyon, gulf of mexico. *Marine and Petroleum Geology* 79, 176–187.
- Moghimidarzi, S., Furth, P. G., Cesme, B., 2016. Predictive–tentative transit signal priority with self-organizing traffic signal control. *Transportation Research Record: Journal of the Transportation Research Board* (2557), 77–85.
- Nelson, P. H., 2010. Sonic velocity and other petrophysical properties of source rocks of cody, mowry, shell creek, and thermopolis shales, bighorn basin, wyoming. *Petroleum Systems and Geologic Assessment of Oil and Gas in the Bighorn Basin Province, Wyoming and Montana, US Geol. Surv. Digital Data Ser., DDS-69-D*.
- Nguyen, S. T., Hoang, S. K., Khuc, G. H., Tran, H. N., et al., 2015. Pore pressure and fracture gradient prediction for the challenging high pressure and high temperature well, hai thach field, block 05-2, nam con son basin, offshore vietnam: A case study. In: *SPE/IATMI Asia Pacific Oil & Gas Conference and Exhibition*. Society of Petroleum Engineers.

- Nour, A., AlBinHassan, N., 2013. Seismic attributes and advanced computer algorithm method to predict formation pore pressure: Paleozoic sediments of northwest saudi arabia. In: IPTC 2013: International Petroleum Technology Conference.
- Oughton, R. H., Wooff, D. A., Hobbs, R. W., O'Connor, S. A., Swarbrick, R. E., 2015. Quantifying uncertainty in pore pressure estimation using bayesian networks, with application to use of an offset well. In: Petroleum Geostatistics 2015.
- Oyana, T. J., Achenie, L. E., Heo, J., 2012. The new and computationally efficient mil-som algorithm: potential benefits for visualization and analysis of a large-scale high-dimensional clinically acquired geographic data. Computational and mathematical methods in medicine 2012.
- Reddy, D., Jana, P. K., et al., 2012. Initialization for k-means clustering using voronoi diagram. Procedia Technology 4, 395–400.
- Riahi, M., Soleymani, H., 2011. Velocity based pore pressure prediction-a case study at one of the iranian south west oil fields. In: 73rd EAGE Conference and Exhibition incorporating SPE EUROPEC 2011.
- Sadeq, Q. M., Yusoff, W. I. W. B. W., 2015. Carbonate reservoirs petrophysical analysis of bai hassan oil field north of iraq. Journal of Bioremediation & Biodegradation 6 (5), 1.
- Saraswat, P., Sen, M. K., 2012. Artificial immune-based self-organizing maps for seismic-facies analysis. Geophysics 77 (4), O45–O53.
- Sarparandeh, M., Hezarkhani, A., 2016. Application of self-organizing map for exploration of rees deposition. Open Journal of Geology 6 (07), 571.
- Sfidari, E., Kadkhodaie-Ilkhchi, A., Rahimpour-Bbonab, H., Soltani, B., 2014. A hybrid approach for litho-facies characterization in the framework of sequence stratigraphy: a case study from the south pars gas field, the persian gulf basin. Journal of Petroleum Science and Engineering 121, 87–102.
- Shahreza, M. L., Moazzami, D., Moshiri, B., Delavar, M., 2011. Anomaly detection using a self-organizing map and particle swarm optimization. Scientia Iranica 18 (6), 1460–1468.
- Sheng, Y.-N., Guan, Z.-C., Xu, Y.-Q., 2017. Quantitative description method for uncertainty of formation pore pressure. Arabian Journal for Science and Engineering, 1–9.
- Soleymani, H., Riahi, M.-A., 2012. Velocity based pore pressure predictiona case study at one of the iranian southwest oil fields. Journal of Petroleum Science and Engineering 94, 40–46.
- Tasdemir, K., Merényi, E., 2009. Exploiting data topology in visualization and clustering of self-organizing maps. IEEE Transactions on Neural Networks 20 (4), 549–562.

- Terzaghi, K., 1925. Principles of soil mechanics, ivsettlement and consolidation of clay. *Engineering News-Record* 95 (3), 874–878.
- Theodoridis, S., Pikrakis, A., Koutroumbas, K., Cavouras, D., 2010. Introduction to pattern recognition: a matlab approach. Academic Press.
- Ugwu, G., 2015. Pore pressure prediction using offset well logs: Insight from onshore niger delta, nigeria. *American Journal of Geophysics, Geochemistry and Geosystems* 1 (3), 77–86.
- Van Buchem, F., Allan, T., Laursen, G., Lotfpour, M., Moallemi, A., Monibi, S., Motiei, H., Pickard, N., Tahmasbi, A., Vedrenne, V., et al., 2010. Regional stratigraphic architecture and reservoir types of the oligo-miocene deposits in the dezful embayment (asmari and pabdeh formations) sw iran. *Geological Society, London, Special Publications* 329 (1), 219–263.
- Wang, Z., Wang, R., Li, T., Qiu, H., Wang, F., 2015. Pore-scale modeling of pore structure effects on p-wave scattering attenuation in dry rocks. *PloS one* 10 (5), e0126941.
- Wild, K., Amann, F., Martin, C., et al., 2015. Some fundamental hydro-mechanical processes relevant for understanding the pore pressure response around excavations in low permeable clay rocks. In: 13th ISRM International Congress of Rock Mechanics. International Society for Rock Mechanics.
- Wohlberg, B., Tartakovsky, D. M., Guadagnini, A., 2006. Subsurface characterization with support vector machines. *IEEE Transactions on Geoscience and Remote Sensing* 44 (1), 47–57.
- Yang, F.-M., Huang, K.-Y., et al., 1991. Multilayer perceptron for detection of seismic anomalies. In: 1991 SEG Annual Meeting. Society of Exploration Geophysicists.
- Zhang, J., 2011. Pore pressure prediction from well logs: Methods, modifications, and new approaches. *Earth-Science Reviews* 108 (1-2), 50–63.
- Zhou, Y., Nikoosokhan, S., Engelder, T., 2017. Sonic properties as a signature of overpressure in the marcellus gas shale of the appalachian basin. *Geophysics* 82 (4), D235–D249.